Image Cover Sheet

CLASSIFICATION	SYSTEM NUMBER
UNCLASSIFIED	502399

TITLE

CHARACTERIZATION OF AN OPTICALLY INTEGRATED MACH-ZEHNDER INTERFEROMETER FOR THE DETECTION OF BIOLOGICAL AGENTS

System Number:

Patron Number:

Requester:

Notes:

DSIS Use only:

Deliver to:

UNCLASSIFIED

DEFENCE RESEARCH ESTABLISHMENT
CENTRE DE RECHERCHES POUR LA DÉFENSE
VALCARTIER, QUÉBEC

DREV – TM–9621

Unlimited distribution/Diffusion illimitée

CHARACTERIZATION OF AN OPTICALLY INTEGRATED MACH-ZEHNDER INTERFEROMETER FOR THE DETECTION OF BIOLOGICAL AGENTS

by

Jean-R. Simard and William E. Lee

April/avril 1997

Approved by/approuvé par

Chief Scientist/Scientifique en chef

14 March '97
Date

SANS CLASSIFICATION

ABSTRACT

The process of environmental monitoring of biological agents is a major concern to the Canadian Forces and to the defence research community in general. The Canadian Integrated Biological Agent Detector System (CIBADS) and the Light Armoured Vehicle Reconnaissance (LAV RECCE) are two projects within the Department of National Defence where smaller, faster, and more sensitive biological detection technologies are of great interest for the integration of an efficient automated monitoring system for biological agents. A device that shows encouraging characteristics for this goal is a biorefractometer based on an integrated Mach-Zehnder interferometer. This document reports initial work to evaluate the capabilities of this device. A model relating the biological sensitivity of the device to its basic electro-optical properties is proposed. Also, the main parameters that may degrade the capacity of the detector are identified and quantified. Off-the-shelf interferometric waveguides were tested experimentally and compared successfully with the proposed model. From these experimental results, it was found that the minimum refractive index change measurable is comparable with the results published by other international scientific teams.

RÉSUMÉ

Le processus de surveillance d'agents biologiques présents dans l'environnement est un sujet important pour les Forces canadiennes et pour la communauté oeuvrant en recherche pour la défense en général. Le système intégré de détection d'agents biologiques (CIBADS) et le véhicule de reconnaissance à blindage léger (LAV RECCE) sont deux projets du ministère de la Défense nationale où une technique de détection biologique plus compacte, plus rapide et plus sensible serait d'un grand intérêt pour l'intégration de systèmes autonomes et efficaces de surveillance d'agents biologiques. Un dispositif possédant certaines caractéristiques encourageantes pour cette application est le bioréfractomètre basé sur un interféromètre Mach-Zehnder intégré. Ce document présente les travaux initiaux visant à évaluer les capacités de ce dispositif. Un modèle reliant les capacités de détection du dispositif à ses propriétés électro-optiques de base est proposé. On a identifié et mesuré les principales variables limitant les performances du dispositif. Des interféromètres intégrés commerciaux ont été testés et les résultats comparés au modèle proposé. Ces résultats montrent que la variation minimale de l'indice de réfraction que l'on peut mesurer est comparable à celle publiée par d'autres équipes scientifiques.

TABLE OF CONTENTS

EXECUTIVE SUMMARY

Overseas military assignments often occur in geographic areas where serious diseases are endemic. The Gulf War presented a scenario of both threat of biological warfare agents and endemic disease. Thus the process of environmental monitoring for biological agents is a major concern to the Canadian Forces.

The most useful monitoring process to date is the Canadian Integrated Biological Agent Detector System (CIBADS). This system, contained in a mobile trailer, includes large volume air samplers and facilities to perform a series of laboratory-style analyses. Although these analyses have proved themselves adequate to detect toxic aerosols, they have the disadvantages to be manually operated and difficult to integrate as automated identification systems. Nevertheless, CIBADS has the capability to incorporate new technologies as they become available, with the overall aim of refining the detection and identification of biological agents to an automated process. Moreover, the development of a faster and automated environmental monitoring technique may make its integration possible on other platforms such as the Light Armoured Vehicle Reconnaissance (LAV RECCE). At present, rapid and automated identification systems do not exist.

A waveguide interferometric immunosensor possesses a number of advantageous characteristics. It is a flow-through system allowing simplified fluidics and sample processing which are amenable to automation. For a developed automated system, the waveguides can be produced through photolithographic technology at a relatively low price. Furthermore, the planar configuration makes the waveguide compatible with other technologies employing micromachined planar glass chips, such as capillary electrophoresis and electro-osmatic pumping. Moreover, multiple biological agent sensing are possible from a single substrate and projected sensitivity is comparable if not better than the current detection technologies.

A theoretical model of an interferometric waveguide immunosensor is proposed in order to relate the biological sensitivity of the device to its basic electro-optical characteristics. The mechanisms which may degrade the capability of the detector are identified and quantified. Commercial off-the-shelf interferometric waveguides were tested experimentally and compared with the proposed model. From these experimental results, it was found that the minimum refractive index change measurable, a parameter dictating the biological agent detection sensitivity, is comparable with the results published by other international scientific teams.

This memorandum is a first Canadian initiative to investigate the capacity of an integrated interferometric immunosensor to improve the ability of the Canadian Forces to

conduct field operations under the threat of use or presence of biological warfare agents as stated in the 1994 Defence White Paper. This work could have impact in several area. Canadian industry is well positioned in micromachining and nanotechnology for chemical and biochemical analysis. The integration of planar waveguides with these technologies can provide new methods of detection and identification through chemical microprocessing and new opportunities for Canadian industry. Canada is a participating member of NATO Panel 7 Project Group 33 on automated biosensors. The work described herein is relevant to NATO Panel 7 in that it presents a novel method of chemical-optical interface.

1.0 INTRODUCTION

The process of environmental monitoring for biological agents is a major concern to the Canadian Forces and to the defence research community in general. The Canadian Integrated Biological Agent Detector System (CIBADS) and the Light Armoured Vehicle Reconnaissance (LAV RECCE) are two projects within DND which involve biological agent detection capabilities. For CIBADS, the process of biological monitoring involves the collection of large volumes of air, the concentration of the contents into water or aqueous buffer, and the subsequent analysis. Typically, with cyclone-style large volume air samplers, approximately one thousand litres of air per minute can be collected and the solid contents deposited in a few millilitres of water or buffer. Then, the resulting samples are subjected to a series of detection-identification analyses based on technologies that include aerosol particle sizing, flow cytometry, immunoassay, gene probe assay, or capillary electrophoresis. This system is adaptable to the incorporation of new technologies as they become available with the overall aim of refining the detection and identification of biological agents to an automated process. Moreover, the development of a smaller, faster, and more sensitive detection technologies would greatly ease the integration of an efficient biological agent monitoring system on platforms like the LAV RECCE vehicle.

Many technological approaches that have potential to achieve smaller, faster, and more sensitive biological agent monitoring employ optical devices in conjunction with surface-bound recognition elements. For these techniques, antibodies (or molecular recognition elements), which have the properties to react with specific analytes (the corresponding bio-elements to detect), are immobilized on optical surfaces. When these surfaces are in contact with the analytes dissolved or suspended in water, reactive bindings occur. Then, these captured analytes are sensed optically by retro-reflection (if the analytes possess flu-

orescence labels) or by refractometry. Surface plasmon resonance (Refs. 1 and 2), resonant mirror (Ref. 3) and fiber based fluorescence biosensing (Refs. 4 and 5) are three examples of these techniques. Although these show greater simplicity than the widely used microplate based methods (e.g. ELISA in Ref. 6), the power requirements and present costs associated with these techniques are restrictive.

In the last few years, a new type of optical transducer has been proposed: the integrated Mach-Zehnder (MZ) biorefractometer (Refs. 7, 8, 9, 10, and 11). This device, as the ones mentioned in the previous paragraph, uses antibody techniques to detect the presence of biological agents. However, the binding reactions in this approach are sensed optically by interferometric measurements. This biorefractometer is built with multi-step processes. First, single mode waveguides are made at the surface of a glass slide using photolithographic techniques in a way that two sections of this device interfere optically (MZ configuration). Secondly, an antibody coating is deposited at the surface of one of the interferometric waveguide sections. When put in contact with the corresponding analytes, the refractive index and thickness of the immobilized coating at the surface of the interferometric arm varies. These variations result in a change of the optical length of the coated waveguide which can be detected with high sensitivity by interferometric measurements. In addition to the high sensitivity, there are two other advantages with this technical approach. First, it is compatible with other technologies employing micromachined planar glass chip, such as capillary electrophoresis and electro-osmatic pumping. Second, the same optical device may be designed to support multiple antibody coatings and to monitor multiple analytes simultaneously.

This memorandum details the initial experiments to evaluate the capabilities of an integrated MZ biorefractometer (minimum measurable refractive index change) discusses

the results and presents recommendations on the direction of future work in integrated optics for biosensors.

This work was carried out at DRES between January and November 1995 under work unit 6EC21: Novel Biosensors for identifying BW agents.

2.0 WAVEGUIDING BASICS

The waveguiding device described in this report is a synthesis of several technologies in the area of integrated optics that began in the 1960s. This chapter provides a theoretical background for the work presented herein on a planar waveguide interferometer. The approach chosen is based on wave formalism from which the local mode theory (Ref. 12, pp. 407-411) is derived. This theory is well adapted to model the experiments shown in Chapter 5.0 (uniform refractive index changes). Subsequently, some modifications are proposed to this theory to make the resulting equations suitable to biological agent detection. Some reservations are stated over the precision of this original approach and potentially better modeling techniques are identified (Ref. 12, pp. 442-459). Finally, the severity of the thermal problem associated with the device is quantified in the last section.

2.1 Fundamentals of an Integrated Mach-Zehnder Interferometer

The device proposed in this document to detect biological agents (BAs) is based on a well-known interferometric design: the Mach-Zehnder (MZ) interferometer (described in the following section). The interferometer splits physically an incident light beam in two beams that travel along two different optical paths before they recombine to produce an interference signal which is dependent on the difference in optical length between the two paths. There are basically two ways to alter the optical length of these paths: change the physical distance traveled or change the refractive index seen by the light beam while traveling through the paths. The device, to be compatible with the techniques used in biological detection, should be fabricated as an optically integrated platform. This platform has the ability to confine all traveling light in optical waveguides of microscopic size. In order to derive a model for the detection capacity of this integrated interferometer, it is

necessary to employ the general concepts of propagation constant, electric field distribution, and single-mode waveguide, which are derived from integrated optic theory. The following two sections provide these basic concepts which are used regularly in this document.

2.1.1 Electromagnetic Mode Treatment for a Step-Index Planar Waveguide

An exact analytical solution for the electromagnetic field structure in single-mode in-diffused waveguides (Ref. 13) as found in the proposed device does not exist. However, the basic features of the behaviour of most dielectric waveguides (including the one described here) can be approximated with the model derived for the step-index planar waveguide (see Fig. 1). This model has the advantage of possessing a complete analytical solution. In the case of the step-index planar waveguide, a general modal form for the field $\mathbf{E}$ [1] in a structure having a constant refractive index in the direction of propagation ($\vec{z}$) can be written as (Ref. 14)

$$\mathbf{E}(x,y,z) = \mathbf{e}(x,y)\exp^{i\beta z}. \qquad [1]$$

In this equation, we intentionally omitted the time dependence because of our exclusive interest to standing wave phenomena and any attenuation along z. The symbols x, y, z are the usual cartesian coordinates, i is the imaginary number, $\mathbf{e}(x,y)$ is the vectorial field now dependent only on the x and y coordinates, and β is the propagation constant. In this equation, we note the appearance of β, a fundamental descriptive parameter of guided waves. This parameter will reappear regularly in the description of the device of interest. With that form, the exact analytical solution for step-index planar waveguide is obtained

[1] Because the magnetic and electric fields obey essentially the same formalism, in most occasions in this document, the word field used alone will represent either of them. However, it is important to keep in mind that two sets of equations (one for the electric field and a second for the magnetic field) are implied with this terminology.

by solving the well-known scalar wave equation (Ref. 12, pp. 240-241),

$$\left(\frac{\partial}{\partial x^2}^2 + k^2 n^2(x) - \beta^2\right) \mathbf{e}(x,y) = 0, \qquad [2]$$

where k is the wave number (defined as the optical angular frequency divided by the

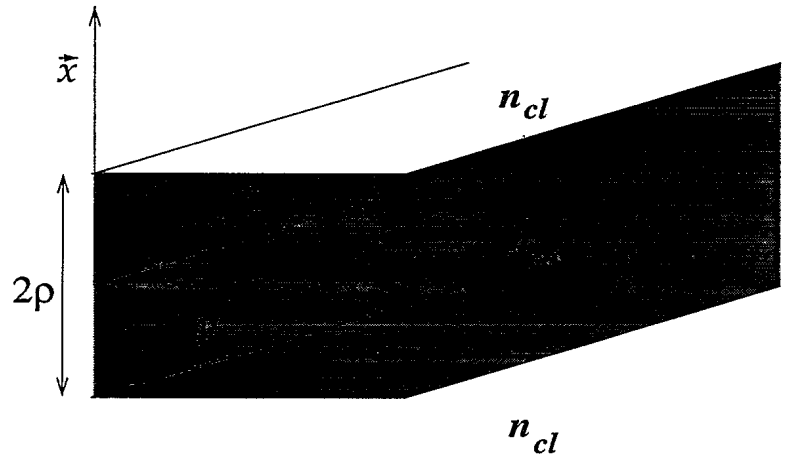

FIGURE 1 – Typical geometry of a symmetric step-index planar waveguide. This structure has the particularity to be infinite in the y direction. The symbols n_{co} and n_{cl} are the refractive indices of the core and the cladding, respectively. The thickness of the waveguiding structure is defined as 2ρ and the zero of the $\vec{x}$ axis is at mid-distance between the two interfaces.

speed of light in vacuum), $n(x)$ is the refractive index distribution and $\frac{\partial}{\partial y} = 0$ (there are no structural changes in the y-direction). This equation is derived from the Maxwell's equations (Ref. 12, p. 590) for the special case of uniform refractive index guide with step-index changes. In addition to complying with this differential equation, the solutions need to satisfy the boundary conditions of continuity for the electric field and its derivative at the dielectric interfaces ($|x| = \rho$). The well-known solutions for this differential equation include two independent classes of field, the transverse electric field TE and the transverse magnetic field TM. These solutions are a complete set (called modes) which reproduce all possible confined electromagnetic field structures in the planar waveguide. One important aspect to visualize with the solution of the scalar wave equation for confined electromagnetic field is

the appearance of discrete solutions. This is a property of bounded space in physics and it implies that in a waveguide structure, a multitude of bounded electromagnetic modes can coexist with their own independent field profiles, and most important, with their own propagation constants β. The presence of multiple modes with their own propagation constants is undesirable for an interferometric device as the one described in this document. That is why it is necessary to base the integrated interferometer on a single-mode waveguiding structure. The set of solutions for the TE modes are shown in Table I [2] (Ref. 12, pp. 242-243). The odd and even modes identify the field solutions in the confined structure where the standing wave crosses zero an odd or even number of times in the x-direction. In these expressions describing the field profile, the parameters are defined as

$$\mathrm{U}_j = \rho(k^2 n_{co}^2 - \beta_j^2)^{1/2}, \quad [3]$$

$$\mathrm{W}_j = \rho(\beta_j^2 - k^2 n_{cl}^2)^{1/2}, \quad [4]$$

$$\mathrm{X} = x/\rho, \quad [5]$$

where the subscripts *co* and *cl* refer to the core and the cladding regions of the waveguide (see Fig. 1). In addition to the field profile, Table I includes the eigenvalue equations derived from the solution of the scalar wave equation (eq. 2) for step-index waveguides. It is these eigenvalue equations which define the possible discrete solutions for $\mathrm{U_j}$ and $\mathrm{W_j}$ [3] which will ultimately determine the possible field profiles (e_y) and propagation constants (β_j) existing in a defined waveguiding structure. To obtain a single-mode waveguide, the thickness of the waveguide ρ is adjusted with the refractive index change ($n_{co} - n_{cl}$) in a way that only one even TE solution is possible for the eigenvalue equations. Waveguides can be readily fabricated to these latter conditions of thickness and refractive index.

[2] Only the expressions for the transverse electric field ($\mathrm{e_y}$) are shown in this table. Readers who would like to obtain all the field expressions should refer to the mentioned reference.

[3] The subscript j in the definitions of $\mathrm{U_j}$ and $\mathrm{W_j}$ identifies these discrete solutions.

TABLE I

Transverse electric (TE) solutions for step-index planar waveguide

Types of solutions	Field profiles (e_y)		Eigenvalue equations
	Core	Cladding	
Even TE	$\frac{\cos(UX)}{\cos U}$	$\frac{\exp(-W\lvert X\rvert)}{\exp -W}$	$W = U \tan U$
Odd TE	$\frac{\sin(UX)}{\sin U}$	$\frac{X}{\lvert X\rvert}\frac{\exp(-W\lvert X\rvert)}{\exp -W}$	$W = -U \cot U$

Note: The definitions of the different parameters are given in eqs. 3, 4 and 5. The expressions for the field in the core and in the cladding are regularly referred to as the confined field and the evanescent field, respectively.

2.1.2 Introduction to the Reciprocity Relation

An additional equation necessary to characterize further the integrated MZ interferometer is the **reciprocity relation**. This equation, based on the modal method for the scalar wave equation (Ref. 12, pp. 644-645), predicts the changes in the propagation constant β for any modifications to the structure of the waveguide. It is based on the definition of the modes existing [4] before and after the change to the waveguide structure ($\mathbf{E}$, β, n and $\bar{\mathbf{E}}$, $\bar{\beta}$, $\bar{n}$). This equation is defined as

$$\bar{\beta}^2 - \beta^2 = k^2 \int_{A_\infty} (\bar{n}^2 - n^2)\, \bar{\mathbf{E}}\, \mathbf{E}\, dA / \int_{A_\infty} \bar{\mathbf{E}}\, \mathbf{E}\, dA, \qquad [6]$$

where k is the traditional wavenumber. Integration is carried out over the whole cross-section of the waveguide (core and cladding) and the expression in the denominator is directly related to the total energy carried by the waveguide. This equation is the basis of the analysis of the transducer presented here and is used below.

[4] Even if this expression is true for the multi-mode waveguide, we will use and discuss it for the case of the single-mode waveguide exclusively.

2.2 Integrated MZ Interferometer Modeling for Biodetection

As mentioned in the previous section, there is no exact analytical solution for the modal characteristics (essentially the mode profile and the propagation constant) of a channel waveguide as the one used to build the integrated MZ interferometer. However, there are numerical methods (Ref. 13, pp. 91-104) to evaluate precisely these characteristics. The manufacturer of the MZ interferometer evaluated in this work has computer software products (Ref. 15) for describing the modal characteristics of a designed waveguide and for providing the protocols to make the waveguides from the glass slides. Although it is possible to obtain quasi-exact values for channel waveguide characteristics throughout numerical methods, the concepts and approaches given in the previous section can be used to obtain close projections on the behaviour of the device. In the following section, the basic equations to evaluate quantitatively the propagation constant when the refractive index is changed uniformly in the evanescent field region are given. This formalism is used directly in Chapter 5.0. Next, Subsection 2.2.2 reports an original approach to relate the propagation constant changes created by biological agent interactions. This new approach, even if very well adapted to the case of BA interactions, needs to be verified experimentally.

2.2.1 Case 1: Uniform Index Change in the Evanescent Field Region

This case describes the experimental testings presented in Chapter 5.0 where liquid exchanges are done in a relatively thick volume over the waveguide. An instructive parameter in this situation is the fraction of power (%**P**) in the cladding region. With this parameter known, preliminary approximations on the sensitivity of the device to detect BAs are possible.

For the case of an uniform refractive index change, the fraction of power in the

evanescent field is derived from the reciprocity relation (eq. 6). First, some simplifications to the reciprocity relation are introduced. These approximations, leading to a solution by the method of perturbations, are possible because the relative quantity of energy contained in the evanescent field region (cladding) is small and because we assume that the field profile in that region changes little with the modification of the refractive index at the surface of the waveguide [5]. With these two assumptions, $\bar{\mathbf{E}}$ is replaced by $\mathbf{E}$ and $\bar{\beta}^2 - \beta^2$ by $2kn_{co}(\bar{\beta} - \beta)$. For this last simplification, we use the basic condition for waveguiding $kn_{cl} < \beta < kn_{co}$, to replace β by kn_{co}. These approximations reduce the reciprocity relationship to

$$\bar{\beta} - \beta = \frac{k(\bar{n}^2 - n^2)}{2n_{co}} \%\mathbf{P}. \qquad [7]$$

This equation implies that the variation of the propagation constant resulting from the change of the refractive index above the waveguide is proportional to the fraction of power in the evanescent field. That equation is verified experimentally in Section 5.4 and, from these results, $\%\mathbf{P}$ will be evaluated (Fig. 13).

2.2.2 Case 2: Localized Refractive Index Change in the Evanescent Field Region

The object of this subsection is to introduce the difficulties associated with the analysis of the integrated MZ interferometer for the detection of BAs. These difficulties take their origin in the small size of the BA. In the previous subsection, the theory proposed for the evaluation of $\%\mathbf{P}$ is adequate because the modification of the refractive index, made by changing the liquid above the waveguide, creates a constant refractive index change in the direction of propagation of the waveguide. This is not the case for the interaction with a BA. The theory used to evaluate $\%\mathbf{P}$ in the previous section is based on the local modes theory (Ref. 12). This theory describes the phase evolution of a guided mode when

[5] This last assumption would be poor if the refractive index change induces large variation in the penetration of the evanescent field, that is if $\%\mathbf{P}$ is more than 1%.

traveling through a waveguide presenting optical non-uniformities. Initially, this theory seems to apply well to the case of the waveguide interacting with the BA, but there is one major weakness with the use of this model: the local mode theory is based on slow non-uniform variations with the distance of propagation. This condition might well be poorly satisfied for the case of the interaction of the BA with the evanescent field. Only one other theoretical approach has been found (Ref. 12, pp. 442-459) to be potentially more adequate to predict the behaviour of a waveguide with non-uniformities comparable in size with the BA, but the formalism used does not give access to the phase information [6]. In default of a better model for now, it has been decided to apply the local mode theory to the case of the interaction between the interferometer and the BA. The reader should keep in mind the previous discussion and should anticipate potential important deviations between experimental results and the predictions of this model.

By using similar simplifications as the ones described to obtain eq. 7, the approximation $n_{co} \simeq n_{gl}$, and by introducing the concept of the local mode theory (Ref. 12), the phase change created by the arrival of a BA ($\Delta\phi_{BA}$) in the region of the evanescent field can be defined as

$$\Delta\phi_{BA} = \int_{BA} \Delta\beta \, dz = \frac{k(n_{BA}^2 - n_w^2)}{2n_{gl}} \%\mathbf{P} \frac{\int_{BA} |e_y|^2 \, dV}{\int_{A_{cl}} |e_y|^2 \, dA}, \qquad [8]$$

where n_{BA}, n_w and n_{gl} are the refractive indices of the BA, the water and the glass, respectively, $\%\mathbf{P}$ is the fraction of power in the evanescent field region which could be measured as shown in Section 5.0. However, the evaluation of the ratio of integrals is difficult because of the spatial distribution of the biological agent, but also, because of the lateral confinement of the evanescent field itself. Nevertheless, for this last aspect,

[6] Theoretical work more adaptable to the prediction of the phase shift caused by the modal interaction with non-uniformities of size comparable with BA might exist in the literature. However, it was not found during the course of this work but its absence did not detract from the overall goals of this effort.

further simplification can be introduced by choosing to represent this lateral confinement by a Gaussian profile of intensity width $2\Delta y$, where Δy can be measured with microscopic imaging techniques. With the lateral description of the field profile defined above and by approximating once more β by kn_{gl}, eq. 8 can be reduced with the definition given in Table I, eqs. 4 and 5 as

$$\Delta\phi_{BA} = \frac{k^2(n_{BA}^2 - n_w^2)(n_{gl}^2 - n_w^2)^{1/2}\,\%\mathbf{P}}{n_{gl}\Delta y\sqrt{\pi}} \int_{BA} \exp(-2k(n_{gl}^2 - n_w^2)^{1/2}x' - \frac{y^2}{(\Delta y)^2})\,dV, \quad [9]$$

where the variable x' has its origin at the interface between the glass and the water (increasing in the water region) and where the integration is done over the whole volume of the BA. This equation, even if its accuracy is compromised by the limit of validity of the local mode theory, has the advantage of giving a projection of the sensitivity of the device to BA detection by taking into account the geometrical aspect of the BA and its position relative to the evanescent field.

Besides the question of validity in using the local mode theory to characterize the integrated MZ interferometer, some basic rules derived from integrated optic theory are readily transferable to the analysis of the effects of using the described interferometer as a transducer. As an example, the distance of penetration of the evanescent field ($\sim 1/k(n_{gl}^2 - n_w^2)^{1/2}$) derived from eq. 4 can be used to compare the region of detection with the size of the BA. This allows the prediction of the efficiency of the device for a specific BA. For example, BA particles that are larger than the effective penetration distance (e.g. bacteria) will be detected with less efficiency (greater minimum detectable mass) than smaller particles (e.g. proteins). A second factor to keep in mind is the effect of adding layers of chemical compounds at the surface of the waveguide to bind the antibodies. Attention has to be given to the change in the evanescent field penetration during that process. Two rules, deduced from waveguide basics, must be applied to minimize the deterioration of the evanescent field

during this operation. First, the refractive index of the coating materials must be equal or higher than the refractive index of the core of the waveguide [7]. This contributes to increase the amplitude of the evanescent field. However, the added layer has to be thin enough to keep a single-mode waveguiding structure. Second, if the first rule cannot be satisfied, it is important to keep the thickness of the coating layer much thinner than the distance of penetration of the evanescent field.

2.3 The Problem of Thermal Instability

In most interferometric measurements, the parameter limiting the sensitivity of the device is the temperature instability which is simply the dependence of the length of the optical paths to temperature changes. Two fundamental parameters dictating the length of the optical path are affected by the temperature: the physical length of the optical path and the refractive index seen by the light beam along that path. The characterization of that phenomenon for an integrated optical fiber interferometer has been reported (Ref. 16) and the results obtained there are directly transferable to the case of the integrated MZ interferometer in a glass slide. From those results, the interferometric phase change $\Delta\phi$ resulting from an uniform temperature difference ΔT between the two optical paths is given by

$$\Delta\phi = \frac{2\pi n l \Delta T}{\lambda}\left[\alpha(1 - \frac{n^2}{2}(p_{11} + 2p_{12})) + \xi\right], \qquad [10]$$

where l is the physical length of the optical path (assumed equal for the two arms), α is the dilatation coefficient, p_{11} and p_{12} are the photoelastic tensor coefficients of glass and ξ is defined as $(1/n)\,(\partial n/\partial T)$. By introducing the values reported (Refs. 16 and 17) for glass waveguides ($\alpha = 13 \times 10^{-6}\,{}^oC^{-1}$, $p_{11} = 0.12$, $p_{12} = 0.27$, $\xi = 6.85 \times 10^{-6}\,{}^oC^{-1}$) and using the parameters describing the MZ characterized in this document ($n \sim 1.5$, $l \sim 1.5$ cm,

[7] For an in-diffused glass waveguide, coating material of refractive index higher than approximately 1.5.

$\lambda = 830$ nm), the phase variation created by a temperature difference ΔT between the two optical paths of the interferometer is given by

$$\Delta\phi = 1.74 \times \Delta T. \qquad [11]$$

This equation states that the temperature difference between the two optical paths of the interferometer needed to create a phase difference of 1^o ($2\pi/360$) is about 1/100 of degree Celsius (0.01 °C). For an application such as the detection of BA, one degree phase change could be many times greater than the signal. Consequently, it is imperative to keep a strict control over the thermal dynamic state of the whole device. That means stabilizing the device and the test liquids at the same temperature. However, there are some aspects in the design of the integrated interferometric BA detector that could be used advantageously to reduce the effect of the inhomogeneity in temperature. First, there is no physical limitation at this time preventing the placement of each interferometric arms at less than 100 μm from each other. This close positioning should minimize the temperature difference between the two interferometric arms. Second, the use of immobilized antibodies already distinguishes chemically one arm from the other. Therefore, it may be advantageous to pass the test liquid over the two interferometric arms. This process would contribute to the equalization of the temperature between the two arms of the interferometer.

A more detailed introduction to these waveguiding formalisms is available with textbooks such as those written by Kolgenik (Ref. 18) or Barnoski (Ref. 19), and in Najafi (Ref. 13) for the specific subject of waveguiding in glass substrate.

3.0 PRINCIPLE OF THE MACH-ZEHNDER INTERFEROMETER

In order to relate the variations of the output signal with the refractive index changes above an arm of the interferometer, it is necessary to express the state of interference of the Mach-Zehnder (MZ) as a function of the propagation constant of the waveguide. To do so, the results of the previous chapter are introduced in the equation describing the interference state of a MZ interferometer. Moreover, the different parameters necessary to completely define the interference state are identified. Finally, the basic conditions for an adequate coherence state is given.

3.1 Basic Descriptions

The MZ interferometric method is well-known (Refs. 20, pp. 27-28, and 21) in the optics community. It is based on amplitude division by which an incoming " monochromatic " beam is split in two, travels along independent optical paths and then is recombined to form the interferometric output signal. In a classical MZ design, the beam splitting is done using a semi-transparent window. For the integrated version, the splitting (and the recombining) is done by waveguide coupling. This is another interferometric phenomenon addressing the energy exchange between two waveguides placed near each other. These regions are identified in Fig. 2 as the Y-junctions. The MZ structure becomes a transducer by correlating the phase difference between the two optical paths with their refractive index changes. The high phase sensitivity of this detection technique is provided by the small dimension of the wavelength associated with the interfering light beams.

The relation between the recombined interferometric signal (I_{rec}) and the phase difference between the two optical paths (ϕ), is given by (Ref. 20, pp. 11-12)

$$I_{rec} = I_1 + I_2 + 2\sqrt{I_1 I_2}\cos(\phi), \qquad [12]$$

where I_1 and I_2 are the light intensities in the two independent paths before recombination. From this equation, two concepts are important. First, the contrast [8] of the interferometric signal for a constant-intensity incoming beam before separation is maximized when the intensity is split equally between the two paths. Consequently, to optimize the sensitivity of the device, it is important to approach this symmetrical configuration. Secondly, the phase difference ϕ is directly related to the propagation constant β introduced in the previous chapter and the length of the optical paths as

$$\phi = \int_{l_1} \beta \, dz - \int_{l_2} \beta \, dz \qquad [13]$$

where the integrals are carried out over l_1 and l_2, the two optical paths traveled by the split beams. For the measurements described in Chapter 5.0 where a phase change $\bar{\phi} - \phi$ is obtained by changing the solution above one arm of the interferometer, the equation relating $\bar{\phi} - \phi$ to the corresponding change in the propagation constant $\bar{\beta} - \beta$ is derived as

$$\bar{\phi} - \phi = (\bar{\beta} - \beta) l \qquad [14]$$

where l is the length of the flow chamber and where $\bar{\beta} - \beta$ is described by eq. 7.

3.2 Relating the Phase ϕ to the Interference Signal

Besides the method for splitting the incoming power between the two optical paths, there are several modeling differences between a free-space and an integrated MZ interferometer. As mentioned in the previous section, the amplitude division for the integrated MZ interferometer is done by what is called mode-coupling. It is a well-known phenomenon in integrated optics where two modes (or more) exchange their energy. For an integrated MZ interferometer, the goal is to design the Y-junctions (see Fig. 2), i.e. the areas where

[8] The contrast is defined as the difference between the maximum (I_{max}) and the minimum (I_{min}) of the interferometric signal divided by their sum.

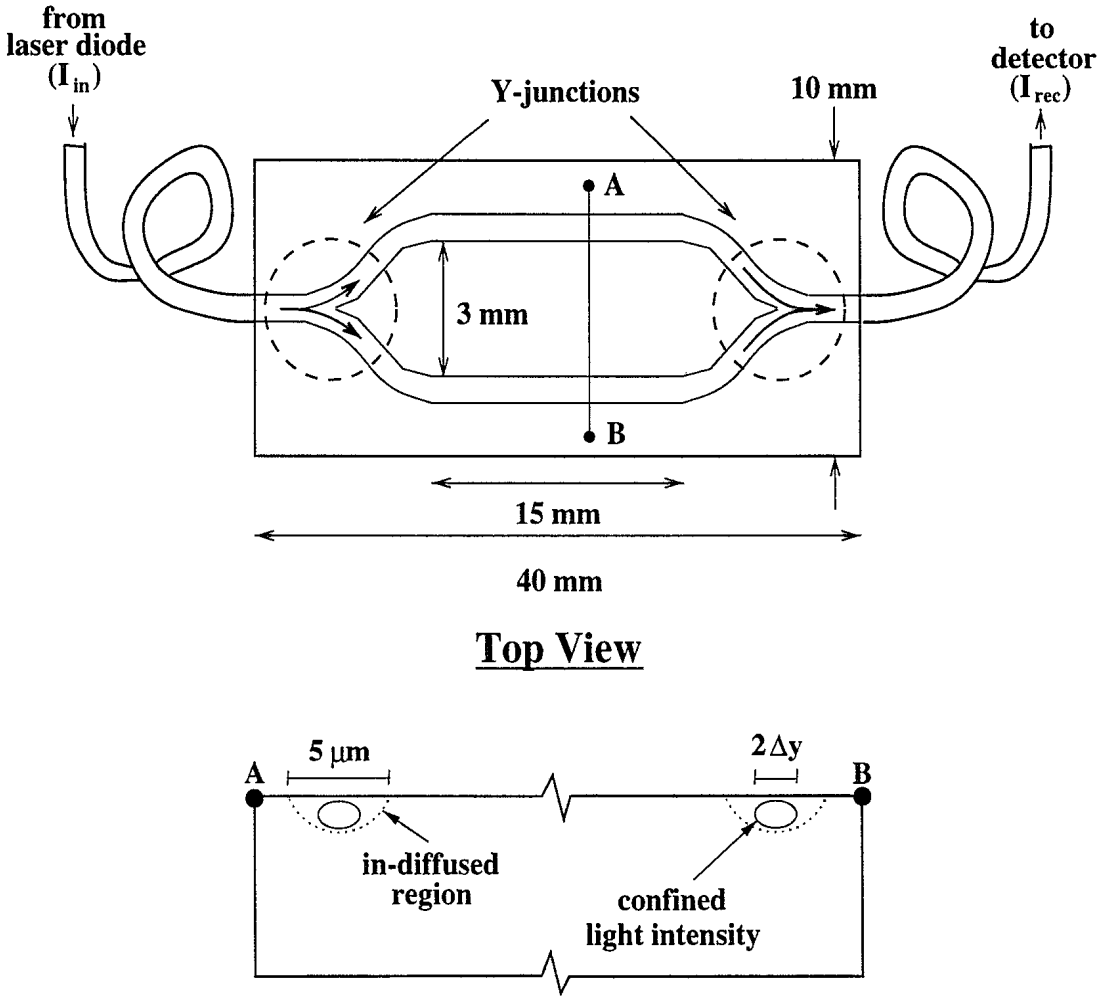

FIGURE 2 – Schematic representation of the integrated Mach-Zehnder interferometer. In the top view, the Y-junctions identify the areas where the initial light beam I_{in} is split between the two optical paths and where they are recombined to form the signal of interference I_{rec}. The interferometer is connectorized with fiber optics (FC connectors) and can easily be coupled to a laser diode and a photodiode with similar connectors. The cross view between the point A and B shows a representative dimension for the in-diffused region and the lateral size in intensity of the confined mode is identified by $2\Delta y$.

the couplings occur, so that half of the incoming intensity I_{in} is directed to each arm. This design is a mature technology in integrated optics. To apply eq. 14 to the experimental results shown in Chapter 5.0, two situations are identified:

1. The phase change observed is small ($\Delta\phi \ll 1$). This is the case when the change in the amplitude of the signal is small in comparison with the difference between the maximum and the minimum interfering signals ($\Delta I_{rec} \ll I_{max} - I_{min}$). In this particular situation, the relation between the phase change and the variation of the recombined signal (ΔI_{rec}) can be described by differentiating eq. 12 with respect to ϕ:

$$\Delta\phi = \frac{-\Delta I_{rec}}{2\sqrt{I_1 I_2}\sin\phi}. \qquad [15]$$

   In this equation, it is important to observe that I_1, I_2 and ϕ are necessary to relate completely the signal variation to the phase change. The method for obtaining I_1 and I_2 is described below. On the other hand, ϕ can only be evaluated by inverting eq. 12. Again, I_1 and I_2 are needed to accomplish this inversion. Nevertheless, two interesting principles are derived from this equation. First, the variation of ϕ with ΔI_{rec} is maximized when the sine is equal to 1 ($\phi = \pi/2$). That occurs when the output signal is at midway between I_{max} and I_{min}, as expected. Second, because $I_1 + I_2$ is equal to the intensity of the incoming beam I_{in} (a constant parameter), then $\sqrt{I_1 I_2}$ and ΔI_{rec} are maximized when $I_1 = I_2$ which supports the comments mentioned in the previous paragraph.

2. The recombined signal change (ΔI_{rec}) observed is not small compared with ($I_{max} - I_{min}$). In this case, the differential approach cannot be applied and the eq. 12 has to

be inverted arithmetically:

$$\Delta\phi = \bar{\phi} - \phi = \arccos\left[\frac{\bar{I}_{rec} - I_1 - I_2}{2\sqrt{I_1 I_2}}\right] - \arccos\left[\frac{I_{rec} - I_1 - I_2}{2\sqrt{I_1 I_2}}\right]. \qquad [16]$$

Again, to solve this equation, it is necessary to know I_1 and I_2. The main difficulty with this equation is the non-unique correspondence between the phase change and the signal change. Depending on the magnitude of the phase change, we could obtain a change in the recombined signal that covers many periods of interference. If the speed at which the phase change occurs is too fast for the instrumentation, it could become difficult to keep track of this number of periods. However, problems associated with large ΔI_{rec} should be negligible for the detection of BA where small signal changes are anticipated.

For the two situations just described, we identified I_1 and I_2 as parameters we need to know to relate $\Delta\phi$ with ΔI_{rec}. A simple method to obtain this information is to change the phase difference between the two optical paths over multiple periods. Through that process, I_{max} and I_{min} are measured. Subsequently, eq. 12 is inverted to find I_1 and I_2 as

$$I_1 = \left(\frac{\sqrt{I_{max}} + \sqrt{I_{min}}}{2}\right)^2, \qquad [17]$$

$$I_2 = \left(\frac{\sqrt{I_{max}} - \sqrt{I_{min}}}{2}\right)^2. \qquad [18]$$

Two techniques have been identified to modify the phase difference over multiple periods. First, large phase changes can be induced by changing the medium above one arm of the interferometer to a higher refractive index. However, this change should be carried out slowly enough to allow the recording of the interference signal variation. For the experimental results shown in Chapter 5.0, this is done by slowly injecting water into one of the flow chambers initially filled with air. A second method is to use the photoelastic properties

of glass [9] to change the refractive index of the waveguides. This technique is less efficient than the first one because large stress needs to be applied to obtain a sufficient gradient between the two optical paths. Furthermore, it has been observed that the limit in stress applied to the device is dictated by the deterioration of the mode coupling state at the Y-junction. A large stress could alter the half-and-half splitting of the initial light power and could seriously reduce the detection efficiency of the device. However, it should be possible to use this technique to create small phase change (less than a quarter of period) in the interference state without deteriorating seriously the mode coupling efficiency at the Y-junctions. This technique could be of great utility to optimize $\sin\phi$ in eq. 15.

3.3 A Note about the Monochromatic Condition

At the beginning of this chapter, when the model of the MZ interferometer was described, we assumed a monochromatic input light beam. In reality, a perfect monochromatic light beam does not exist (even a laser beam is not perfectly monochromatic). In practical situations, this condition is reduced to a limit of validity relating the optical path difference between the two arms of the interferometer and the spectral width of the input light. This relation, deduced from the well-known equation $\Delta t \cdot \Delta\nu = 1$, states that we have a good interferometric coherence when

$$\Delta\lambda \ll \frac{\lambda^2}{n\Delta l}, \qquad [19]$$

where $\Delta\lambda$ is the spectral width of this incoming light, λ is the centre wavelength of this incoming light, and $n\Delta l$ is the optical path difference between the two interferometric arms. For a symmetrical integrated MZ interferometer where $n\Delta l$ is zero initially, as those evaluated in this document, this condition of coherence is easily satisfied. Even with the optical

[9] The photoelastic properties relate the refractive index and the stress existing in the material. Yariv (Ref. 17) and Heaton (Ref. 16) give a good description of that phenomenon in glass.

path difference changing because of the detection process, it is difficult to imagine this difference being much more than 10 μm. According to this limit, the spectral width of the input light has to be much smaller than 50 nm to satisfy the monochromacity condition. Nevertheless, to be sure to satisfy that condition experimentally, an optical isolator was attached to the laser diode (the input light source) used to obtain the results shown in Chapter 5.0. This precaution reduces the spectral width of the laser diode from approximately 5 nm to less than 1 nm (Ref. 22).

4.0 DESCRIPTION OF THE EXPERIMENTAL PROCEDURE

In order to verify the capability of the integrated MZ interferometer to act as a transducer for the antibody technology, an experimental setup was designed. The ultimate goal of this design was to measure the percentage of energy carried by the interferometer in the cladding region (**%P**). The first section of this chapter describes the two different systems forming this experimental setup and the second section describes the procedures followed to prepare the solutions of different refractive indices used to test the MZ interferometer.

4.1 Description of the Experimental Setup

As mentioned in Section 2.2, the measurement of **%P** leads to a quantitative evaluation of the evanescent field profile. This experimental design involved the integration of two main systems, as described below.

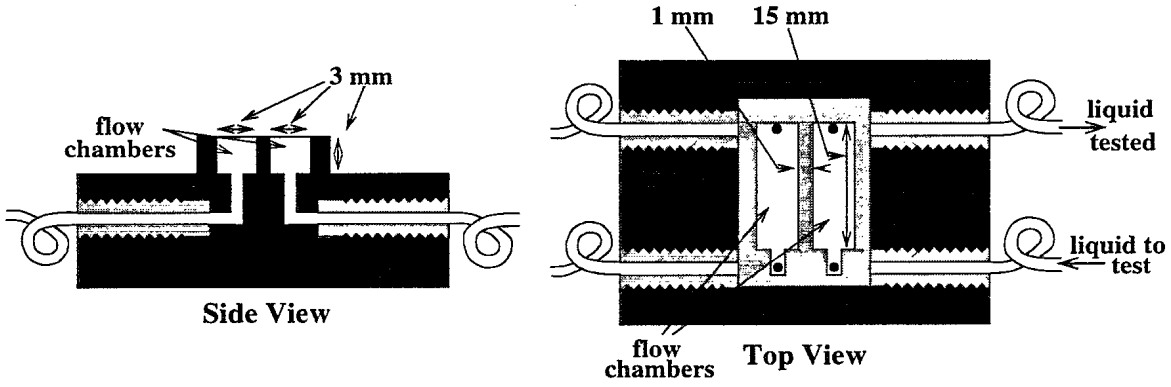

FIGURE 3 – Schematic representation of the flow chamber used to change the liquid at the surface of the interferometer's arms

First, there was the fluidic system. This system was designed to change independently the solutions over the two arms of the interferometer. It was composed principally of a flow chamber (see Fig. 3) made of Teflon where mini-structures have been cut to carry the

different liquids to test. This flow chamber was placed on a θ-X-Y-Z positioning system (see Fig. 4). The positioning system was used to carefully align the arms of the interferometer with the flow chambers. When the alignment was done, the two flow chambers were placed in contact with the interferometer and mechanical pressure was applied to obtain a seal. A system of tubes allowed the exchanges of liquid in the flow chambers.

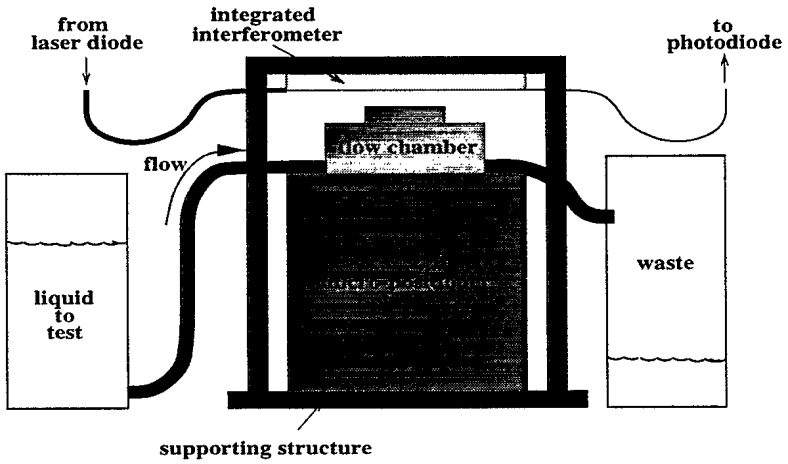

FIGURE 4 – Schematic representation of the positioning system. This apparatus was used to align the flow chamber with the interferometer.

Second, there was the electro-optical system (see Fig. 5). It was composed of a laser diode connected to a single-mode fiber ending with a FC connector [10]. To stabilize the optical power output and to maximize the spectral purity of the laser diode, three components were connected with this light source: a low-noise current controller, a temperature controller and an optical isolator (see Table II for more information on the experimental instrumentation). Another single-mode fiber with the corresponding FC connector was coupled to the integrated MZ interferometer. After passing through the interferometer, a second set of single-mode fibers carried the interference signal to a photodiode which converted the optical signal into an electrical one. To facilitate the detection process, the laser

[10]The recent arrival of efficient single-mode fiber optic connectors made possible the introduction of a modular approach in the design of this experimental setup. This approach has the advantage of making each module independent and easily interchangeable.

diode was modulated at a frequency of 1 kHz with a wave generator to allow the implementation of a synchronous detection technique. This detection technique was performed with a lock-in amplifier which amplifies the electric current provided by the photodiode. Finally, the amplified analog signal was digitized by an A/D converter board at a specific sampling rate (100 Hz) and stored on a computer's hard drive.

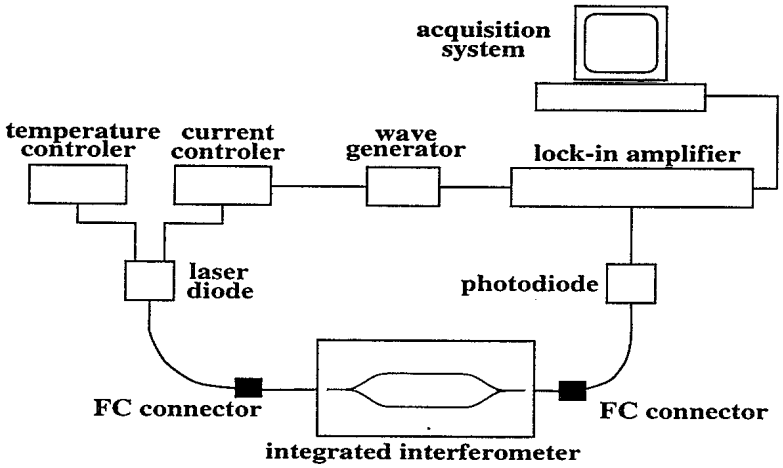

FIGURE 5 – Schematic representation of the electro-optical system. This system measures the variations of the recombined signal in response to any changes in the liquid composition above the interferometer's arms.

4.2 Preparation of the Liquid Solutions for Testings

To gradually modify the refractive index of the liquids to test, double distilled water and analytical grade ethyl alcohol (Sigma Chemical Co., St Louis, MO) were employed. The refractive indices of these solutions were evaluated by volume ratios [11]. The overall refractive index of a solution of water and ethyl alcohol (n_{w+et}) and the error associated with the imprecision of the measurements of the volumes (Δn_{w+et}) were:

$$n_{w+et} = \mathcal{F}_w \times n_w + \mathcal{F}_{et} \times n_{et}, \quad [20]$$

$$\Delta n_{w+et} = \Delta\mathcal{F} \times n_{et} - \Delta\mathcal{F} \times n_w, \quad [21]$$

[11] We assumed a linear correspondence between the volume ratios and the resulting refractive indices.

TABLE II

Instruments used to characterize the Mach-Zehnder interferometer

Component	Manufacturer	Model	Characteristics
Laser diode	Seastar Optic Inc. [a]	PMSEI0830LT015MD-G	SM, OI and TS $\lambda = 830nm$
Photodiode	Seastar Optic Inc. [a]	CP12LP0830PD2101	λ: 600-900 nm, 300 MHz cutoff
Mach-Zehnder interferometer	Guided Wave Technologies Inc. [b]	Custom design	Single mode (830 nm) Connectorized
Thermoelectric controller	Seastar Optic Inc. [a]	TC-5100	Stability: $\pm.01°C$
Current controller	Seastar Optic Inc. [a]	LD-1000	TTL Modulation capacity
Lock-in amplifier	EG&G [c]	5210	
Function generator	Hewlett Packard [d]	8111A	up to 20 MHz
A/D converter board	Data Translation [e]	DT 2837	16 bits conversion
Computer	NEC [f]	386 (25 MHz)	Window 3.1 (OS)
θ-X-Y-Z micro-positionner	Optikon Corporation Ltd. [g]	M4034M and M10000	

[a] 316 Second Ave. S., Seattle, WA 98104. [b] 481, Victoria Ave., Westmount, Quebec, H3Y 2R3. [c] 1182, South Service Road West, Oakville, Ontario, L6L 5T7. [d] 2670, Queensview Dr, Ottawa, Ontario, K2B 8K1. [e] 100, Locke Dr, Marlborough, MA. [f] Mississauga, Ontario. [g] 410, Conestogo Rd, Waterloo, Ontario, N2L 4E2.

Note: The abbreviations SM, OI, TS for the laser diode characteristics stand for single-mode, optically isolated and temperature stabilized, respectively.

where $\mathcal{F}_w$, n_w and $\mathcal{F}_{et}$, n_{et} are the volume fractions and the refractive indices of the water and the ethyl alcohol, respectively. The symbol $\Delta\mathcal{F}$ represents the largest error when evaluating the volume fraction (water or ethyl alcohol). This equation is derived from the fundamental rule $\Delta\mathcal{F}_w$ = - $\Delta\mathcal{F}_{et}$. The refractive indices of water and ethyl alcohol have been taken from the CRC handbook (Ref. 23) as: $n_w = 1.33262$ and $n_{et} = 1.35885$ ($24°C$). These solutions were made first by mixing 250 mL of water with 250 mL of ethyl alcohol. Volumes were measured using a 100 mL graduated cylinder having a graduation of 1 mL. Subsequently, 30 mL of this solution, taken with the same cylinder, were combined with the

TABLE III

The different solutions used to change gradually the refractive index

$\mathcal{F}_w$	$\Delta\mathcal{F}_w$	$\mathcal{F}_{et}$	$\Delta\mathcal{F}_{et}$	n_{w+et}	Δn_{w+et}
0.50	.010	.50	.010	1.3457	0.0005
0.30	.0093	.70	.019	1.3510	0.0005
0.40	.013	.60	.019	1.3484	0.0005
0.45	.016	.55	.021	1.3471	0.0006
0.48	.017	.52	.021	1.3463	0.0006
0.49	.018	.51	.022	1.3460	0.0006

Note: The interfering signal changes are measured when one solution is replaced with another one.

volume of ethyl alcohol corresponding to the desired solution. The volume of ethyl alcohol was measured with a 20 mL graduated cylinder (.2 mL graduation) or a 10 mL cylinder (.1 mL graduation). Table III shows the volume fractions and the associated errors of the different solutions used to test the device. This table also shows, by using eqs. 20 and 21, the refractive indices and the anticipated errors on the refractive indices of the resulting solutions. The water-ethyl alcohol solutions were mixed, covered, and allowed to stand for at least two hours before testing. This procedure allowed the solutions to equilibrate to the same temperature.

5.0 EXPERIMENTAL RESULTS

In the previous chapters, a model was introduced to characterize the integrated Mach-Zehnder (MZ) interferometer. In this chapter, experimental results that were performed to verify the validity of the model are presented. First, the maximum and the minimum signals of interference were evaluated. Then, the output signal changes associated with the variations of the refractive index over one arm of the interferometer were recorded. From these measurements, the minimum refractive index variation measurable was evaluated and the fraction of light power in the evanescent field region, a parameter leading directly to a measure of the evanescent field penetration, was estimated for the interferometer tested.

5.1 Evaluation of the Maximum and the Minimum Signal of Interference

As mentioned in Section 3.2, characterizing a MZ interferometer necessitates the knowledge of the maximum (I_{max}) and the minimum (I_{min}) signals of interference. To obtain this information, a 1.5 mL syringe was used to slowly fill one of the flow chambers, that initially contained air, with water (the second chamber was already filled with water). The flow chamber was of small enough diameter that the water formed a "plug" that moved forward under pressure from the syringe and increased the refractive index above the waveguide. Thus it was possible to monitor a gradual change of phase in the interferometer. The large refractive index change created by replacing air with water along the 15 mm length of the flow chamber was sufficient to shift the interferometer through several periods of phase. Moreover, the water movement was reversible. It was then possible to obtain the reverse phase change by extracting the water from the flow chamber with the same syringe. The interference signal change obtained with this technique is shown in Fig. 6. This plot

shows the reversible property of the operation. However, strong differences between the amplitude of the two first interference lobes and the third one are observed. Two possible reasons explaining this disparity are an imperfect covering made by the flow chamber in the Y-junction regions or waveguide characteristic inhomogeneities in the direction of propagation. Nevertheless, approximate values for the maximum and minimum of interference can be derived from this graph by using the averaged values over the three maximums and minimums of interference for the injection and the extraction processes. With this averaging approach, these values have been estimated as 5.5 and 2.5, respectively. With these results and eqs. 17 and 18, I_1 and I_2 are evaluated to 3.9 and 0.2, respectively. This result shows that the optimal condition $I_1 = I_2$ was far to be satisfied for these measurements. Therefore, an improvement of the following results is anticipated with a better control on the amplitude splitting between the two interferometer arms. Table IV reports the principal settings used to obtain these results. During the experimental measurements, a dependence between the

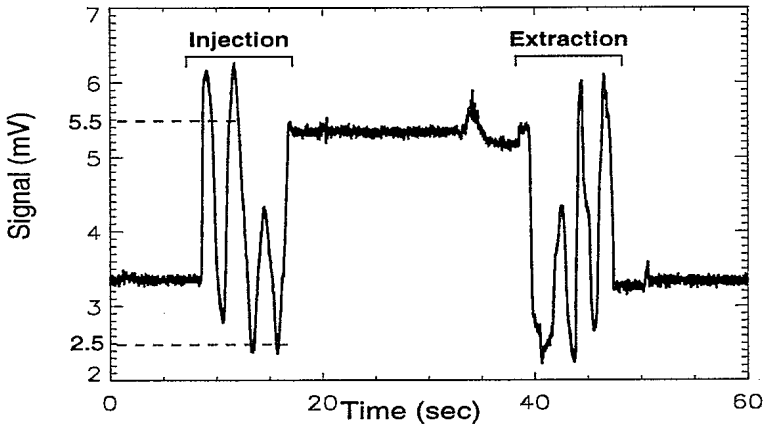

FIGURE 6 – Interference signal at the output of the integrated MZ interferometer over multiple periods. The phase change was made by slowly injecting water (first group of interference signal) in the flow chamber initially filled with air. The second group of interference signal was obtained by slowly extracting the liquid from the flow chamber, replacing water by air. This method allowed the evaluation of the maximum (I_{max}) and minimum (I_{min}) signals of interference which have been approximated to 5.5 and 2.5, respectively.

TABLE IV

Basic parameter settings for the experimental acquisitions

	Parameters	Settings
Lock-in amplifier:	Amplification scale	10 mV (full scale)
	Time constant	3 ms
	Current to voltage conversion gain	10^6 V/A
	Modulation carrier filtering	Bandpass
	Line filter	f and 2f
	Averaging	12 db slope and high stability
Laser diode:	Modulation	Square
	Current (peak)	80 mA
	Temperature	25 °C
Photodiode:	Current divider	1000 times
A/D conversion:	Rate	100 Hz
	Duration	160 s
	Gain	1

state of interference and the applied pressure to seal the flow chamber with the integrated interferometer was observed. We believe this effect is related to a change of the refractive index with the variation of the stress in the glass. To a lower extent, this stress variation may also modify the coupling state in the Y-junction which may modify the divided light intensity between the two arms. To minimize this effect on the characterization of the interferometer, the evaluation of the maximum and minimum of interference was done just before the measurements of the interference signal changes associated with the solution exchanges in the flow chamber (see following section). Between these two experimental steps, only slight changes to the pressure between the flow chamber and the interferometer were done to position the interference state in an optimum way between the maximum and the minimum.

5.2 Refractive Index Changes vs Interference Signal Variations

This section reports the main experimental results characterizing the integrated MZ interferometer as a refractive index sensor. To acquire this information, water-ethyl alcohol solutions of specific refractive indices (see Section 4.2 for the procedure followed for their preparation) were successively injected into one of the flow chambers, directly pushing out the previously injected solution, while measuring the interference signal changes. The other chamber contained water during the whole process. The configuration of the experimental setup was similar to the one described in Table IV with the following two exceptions:

- The lock-in amplifier time constant was set to 1 second.
- The injection of the new solution was done one minute after the start of the acquisition process with a 25 mL syringe (injection time shorter than 3 seconds).

The whole process, including the six exchanges of solutions, was performed in less than 1 hour. The order followed for the injections of the solutions is shown in Table V. The figures identified in parentheses correspond to the plots of the signal changes obtained during the specified injected solution procedures. In this table, only the fractions of water are shown (% ethyl alcohol = 100 - % water). Only the best graphical results obtained for the six successive injected solutions are presented. In many occasions (data not shown), fluctuations in the interference signal were observed. Some possible sources of these fluctuations have been identified as surrounding temperature fluctuations, temperature differences between the injected solutions or presence of particles in suspension interacting with the evanescent field. It is anticipated, for the results plotted, that temperature fluctuations (from the surroundings or between the different injected solutions) are responsible for the variations between the final phase of a plot and the initial phase of the following plot.

TABLE V

Procedure followed for the different solution exchanges

Initial solutions	Final solutions	Corresponding figure
100% water	50% water	Fig. 7
50% water	30% water	Fig. 8
30% water	40% water	Fig. 9
40% water	45% water	Fig. 10
45% water	48% water	Fig. 11
48% water	49% water	Fig. 12

For the six injected solutions, the recombined signals were measured before (I_{rec}) and after ($\bar{I}_{rec}$) the moment of the solution exchanges. To reduce the transitional effects associated with the injections, I_{rec} and $\bar{I}_{rec}$ were measured by extrapolating straight lines fitted with the values of the interference signals sufficiently before and after the moment of the solution exchanges. These values for I_{rec} and $\bar{I}_{rec}$ are used in the next section to evaluate the corresponding phase changes. In addition to the measurement of I_{rec} and $\bar{I}_{rec}$, the background noise level is evaluated in Fig. 12. The standard deviation of this noise was measured by fitting a straight line over the acquired points sufficiently after the moment of the injection (the value of the background noise was determined to be 0.003 mV). One can note the spiked structure in the interference signal which is included in the noise evaluation. It is believed this feature takes its origin in the electronics of the detection system.

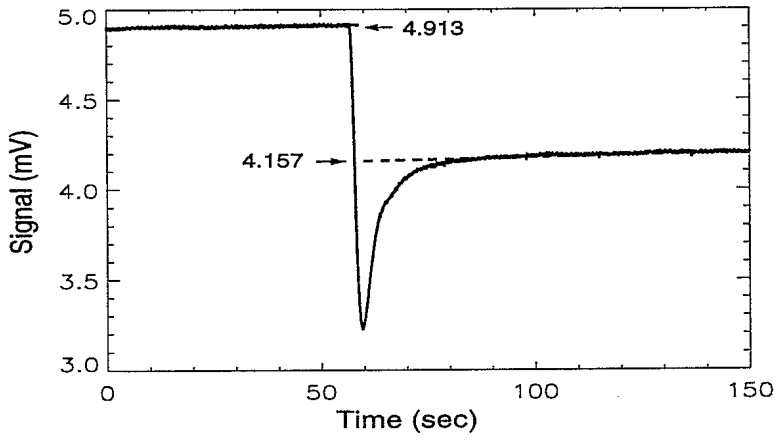

FIGURE 7 – Interference signal change when a 50% water-50% ethyl alcohol solution was injected in the flow chamber initially filled with water. The injection was done approximately 60 seconds after the beginning of the acquisition. The values identified on the graph are the initial and final interference signals evaluated numerically. One can note the noise reduction associated with the use of a larger time constant when compared with Fig. 6.

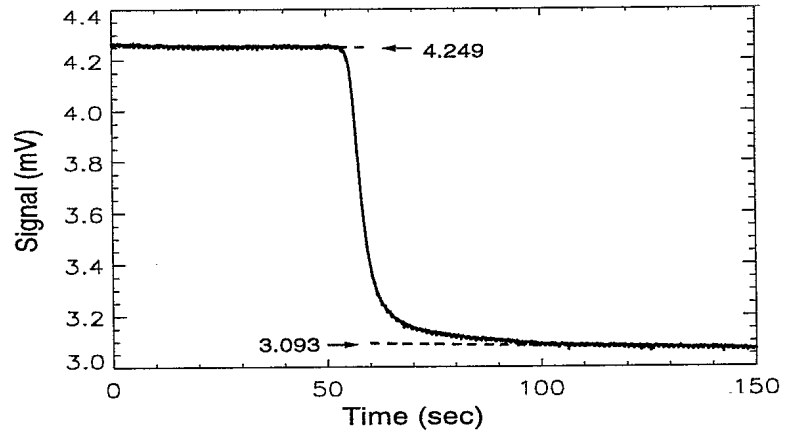

FIGURE 8 – Interference signal change when a 30% water-70% ethyl alcohol solution was injected in the flow chamber initially filled with a 50% water-50% ethyl alcohol solution. The injection was done approximately 60 seconds after the beginning of the acquisition. The values identified on the graph are the initial and final interference signals evaluated numerically.

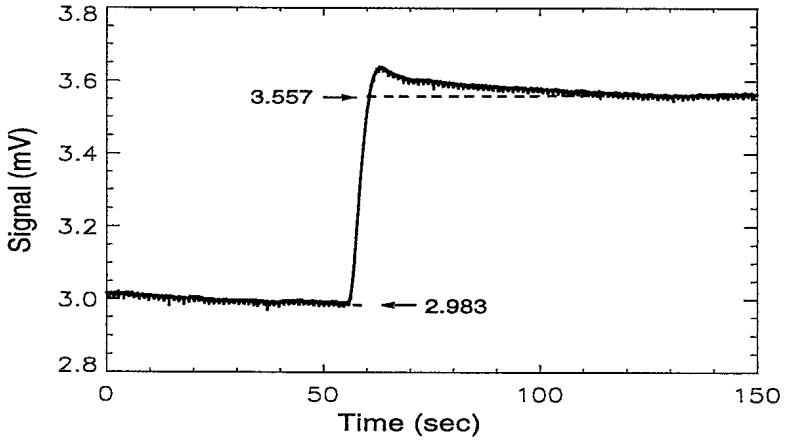

FIGURE 9 – Interference signal change when a 40% water-60% ethyl alcohol solution was injected in the flow chamber initially filled with a 30% water-70% ethyl alcohol solution. The injection was done approximately 60 seconds after the beginning of the acquisition. The values identified on the graph are the initial and final interference signals evaluated numerically.

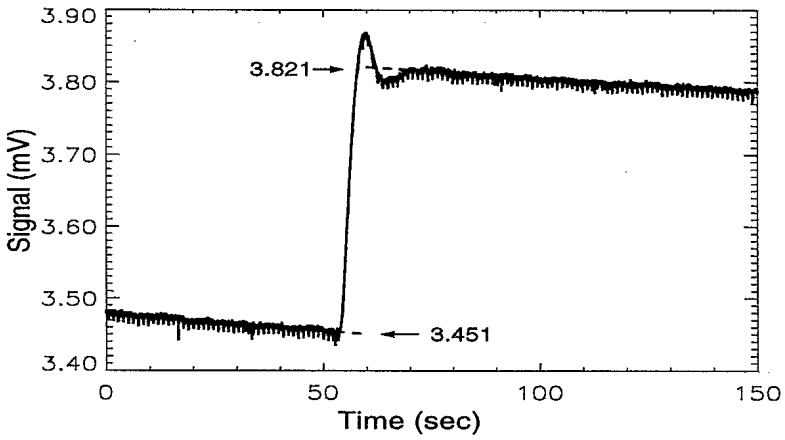

FIGURE 10 – Interference signal change when a 45% water-55% ethyl alcohol solution was injected in the flow chamber initially filled with a 40% water-60% ethyl alcohol solution. The injection was done approximately 60 seconds after the beginning of the acquisition. The values identified on the graph are the initial and final interference signals evaluated numerically.

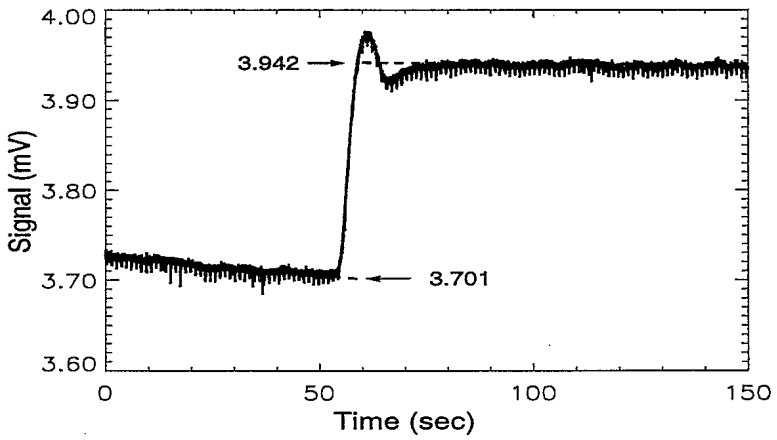

FIGURE 11 – Interference signal change when a 48% water-52% ethyl alcohol solution was injected in the flow chamber initially filled with a 45% water-55% ethyl alcohol solution. The injection was done approximately 60 seconds after the beginning of the acquisition. The values identified on the graph are the initial and final interference signals evaluated numerically.

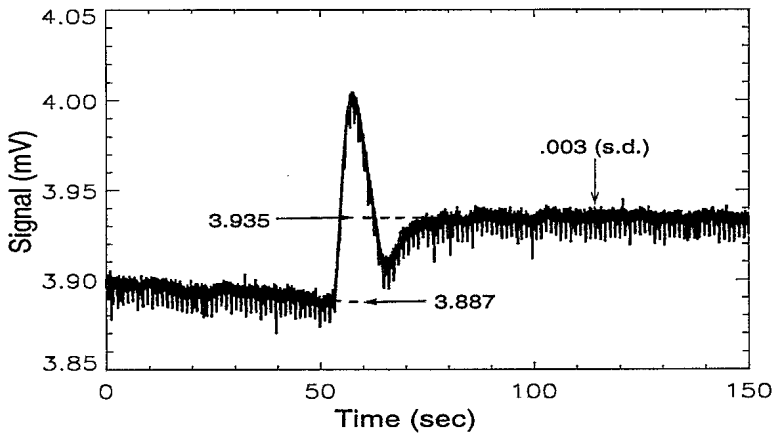

FIGURE 12 – Interference signal change when a 49% water-51% ethyl alcohol solution was injected in the flow chamber initially filled with a 48% water-52% ethyl alcohol solution. The injection was done approximately 60 seconds after the beginning of the acquisition. The values identified on the graph are the initial and final interference signals evaluated numerically. Also, the background noise, the standard deviation of the signal away from the moment of the injection, was evaluated to be 0.003 mV.

5.3 Minimum Refractive Index Change Measurable

The minimum refractive index measurable Δn_{noise} is the value of the refractive index change corresponding to the noise level observed when measuring the signal of interference (ΔI_{rec}^{noise}). Because this characterization was done for small signals, a linear relation as in eq. 15 was assumed between the refractive index change and the variation of the recombined signal. With this approach, Δn_{noise} is easily derived by linear extrapolation as

$$\Delta n_{noise} = \frac{\Delta n \times \Delta I_{rec}^{noise}}{\Delta I_{rec}}, \qquad [22]$$

where Δn and ΔI_{rec} are the refractive index change and the corresponding interference signal change for small signal variation as shown in Fig. 11. The refractive index change associated with this plot is found in Table III by subtracting the refractive index for the solution 45% water + 55% ethyl alcohol from the one corresponding to the solution 48% water + 52% ethyl alcohol. This gives a refractive index change of .0008. On the other hand, the variation of the interference signal corresponding to this refractive index change is directly given by the plot in Fig. 11 as 3.942-3.701 mV (0.241 mV). The noise level has been evaluated, as described in the previous section, to 0.003 mV. With these three numerical values introduced in eq. 22, the minimum refractive index measurable limited by the interference signal noise is given by

$$\Delta n_{noise} = 1 \times 10^{-5}. \qquad [23]$$

However, mainly because of the imprecision over the refractive index of the water-ethyl alcohol solutions, this minimum refractive index change measurable may be as twice larger than the value given.

5.4 Evaluation of the Fraction of Power in the Evanescent Field Region (%P)

In this section, the experimental results shown in Section 5.2 and the corresponding refractive index changes given in Table III are introduced into the model developed in Chapters 2.0 and 3.0 in order to evaluate the fraction of optical power localized in the evanescent field region. First, the phases before (ϕ) and after ($\bar{\phi}$) the solution exchanges over one arm of the interferometer are evaluated with eq. 12. For all the solution exchanges, except the first one (100% water replaced by 50% water solution), the phase variations are small enough to create no ambiguities on the initial and final phase values. But in the case of the first injected solution, it is possible to demonstrate by comparison with the other phase changes and by interpreting the developed model that the final phase ($\bar{\phi}$) for this first injected solution is given by (2π -$\tilde{\phi}$) where $\tilde{\phi}$ is obtained by inverting eq. 12 where I_{rec} is replaced by $\bar{I}_{rec}$. The refractive index before (n) and after ($\bar{n}$) the solution exchanges were derived from Table III. Finally, eqs. 7 and 14 are combined to relate the phase variations to the refractive changes which allows the calculation of the fraction of power in the evanescent field region as

$$\%\mathbf{P} = (\bar{\phi} - \phi) / \left(\frac{kl(\bar{n}^2 - n^2)}{2n_{gl}} \right), \qquad [24]$$

where n_{co} is approximated by n_{gl}, the refractive index of glass. Table VI gives all the numerical values used in this evaluation and Fig. 13 shows the plot of the previous equation where the slope is the fraction of power in the evanescent field region.

TABLE VI

Measured and evaluated interference states

Water fraction changes	I_{rec}	ϕ	$\bar{I}_{rec}$	$\bar{\phi}$	$\bar{\phi}-\phi$	n	$\bar{n}$	$\frac{kl(\bar{n}^2-n^2)}{2n_{gl}}$
1.0 → .50	4.913	0.917	4.157	4.817	3.900	1.33262	1.3457	1300
0.50 → 0.30	4.249	1.404	3.093	2.220	0.812	1.3457	1.3510	540
0.30 → 0.40	2.983	2.316	3.557	1.870	-0.445	1.3510	1.3484	-270
0.40 → 0.45	3.451	1.946	3.821	1.690	-0.255	1.3484	1.3471	-130
0.45 → 0.48	3.701	1.772	3.942	1.609	-0.162	1.3471	1.3463	-81
0.48 → 0.49	3.887	1.646	3.935	1.614	-0.032	1.3463	1.3460	-27

Notes: The experimental values measured (I_{rec}, $\bar{I}_{rec}$) are derived from the plots found in Figs. 7, 8, 9, 10, 11 and 12. The other values are derived from the theory described in Chapters 2.0 and 3.0 and with $n_{gl} = 1.49$.

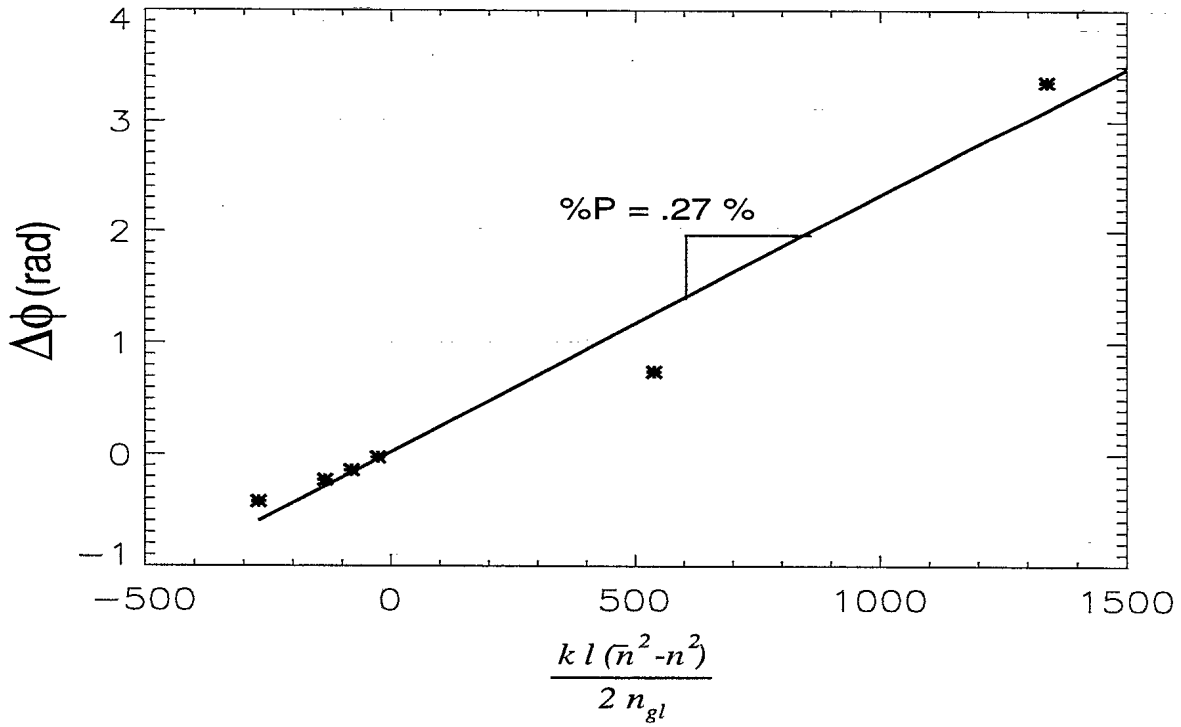

FIGURE 13 – Plot of the phase changes corresponding to the variations of the refractive index factor (eq. 24). The slope of the straight line fitted with these points is the fraction of optical power in the evanescent field region which is evaluated to 0.27%.

6.0 DISCUSSION

In order to evaluate the capability of the integrated Mach-Zehnder (MZ) interferometer to be used as a biological agent (BA) detector, a model including several basic relations is proposed. Several important parameters, such as the propagation constant β, the shape of the evanescent field **E**, and the optical power in the evanescent field region **%P** are quantified for the case of an uniform refractive index change over one arm of the interferometer. These relations, in association with the equations dictating the interference state of the interferometer, were tested experimentally with success with off-the-shelf integrated MZ interferometers. From these experiments, **%P** is evaluated to be 0.27% which is in agreement with the nominal optical power found in the evanescent field region for in-diffused glass waveguide. Also, the minimum refractive index variation measurable with this device was evaluated to be 1×10^{-5}. Considering the length of the flow chamber, the wavelength used for these measurements, and the noise source present in the electronics of detection (the spiked structures observed in the base line in Fig. 12), this limit of detection is advantageously comparable with the results obtained by other scientific teams working on similar devices (Refs. 11 and 24). Furthermore, a modified version of the equation relating the phase change of the interferometer with an uniform variation of the refractive index over one arm of the interferometer is proposed (eq. 9). This version attempts to relate the change of the interference state resulting from the interaction of a single BA with the evanescent field by taking into account the size and shape of this BA. It is understood, because of the limit of validity of the theoretical approach proposed to obtain this relation (particularly the difficulty to relate the effects of dispersed small particles and a model based on slow variations of the electromagnetic field [12]), that the predictions issued from this equation

[12]It is well-known that the electromagnetic field needs an interaction length much greater than its wavelength to rearrange its field configuration to take into account any changes in the optical characteristics of

may be overvalued. Nevertheless, we believe this equation has valuable scientific merit because it relates the shape and size of the evanescent field to the shape and size of the BAs.

Besides the basic characterization of the integrated interferometer, two conditions are identified as important for an acceptable performance of the device. First, there is the monochromatic condition (eq. 19) for a maximum amplitude of interference. In Section 3.3, it was established that the electro-optic components chosen satisfy well this monochromatic condition. Secondly, and most important, Section 2.3 identifies the thermal instability as one of the critical perturbations to minimize for an optimized detection capability of the transducer. It was estimated that a temperature difference of 0.01 ^oC between the two arms of the tested interferometer is sufficient to create a phase variation of 1^o. When considering that the phase variation associated with the interaction of several BAs is much smaller than 1^o, it is imperative that special attention be given to reduce any sources of thermal instabilities. In many occasions during the experimental measurements, the observed fluctuations were related to this thermal instability. For future experiments, two design features should be included in the experimental setup to reduce this effect: fabricating the two arms of the interferometer as close as possible to each other and passing the test liquid over both arms of the interferometer [13]. Also, stabilizing the interferometer and the test liquid at the same temperature may be advantageous.

Finally, it was identified in Section 3.2 that the optimum sensitivity of the device was obtained when the initial phase difference for an optimum interference state is about $\pi/2$. This condition may be difficult to achieve for the complete BA detector where multiple coatings applied asymmetrically over the two arms of the interferometer would change the

the surroundings. One direct effect of this property for the case of BA detection, when using the proposed relation, is to overestimate the effect of one BA cell on the propagation constant of the confined mode.

[13]This procedure implies that one arm has been sensitized for the test liquid (e.g. antibodies coating).

interference state to an unpredictable value. A method to overcome this difficulty was identified. It was observed, during the course of the experiments, that a small stress applied on the integrated interferometer was sufficient to vary the interference state over multiple cycles. Therefore, it should be possible to optimize the condition of interference of the final biodetector by carefully applying mechanical pressure on the device. However, this approach may be inapplicable for a biodetector supporting more than one interferometer.

7.0 CONCLUSIONS

This memorandum is the first Canadian initiative to evaluate the potential of an integrated Mach-Zehnder (MZ) interferometer for biological agent (BA) detection. First, a model including the fundamental equations relating an uniform refractive index change over one arm of the interferometer with its overall interference state was established. With this model, the fraction of light power in the evanescent field region, an important parameter characterizing the capacity of the proposed device to act as a biological agent detector, was evaluated experimentally with off-the-shelf integrated MZ interferometers. Also, the minimum measurable refractive index change over one arm of the interferometer was evaluated experimentally to be 1×10^{-5}. Considering the characteristics of the experimental setup, this limit of detection is comparable with the results obtained by other scientific teams. Furthermore, the thermal instability is identified as an important undesirable phenomenon and different measures to reduce its effect on the performance of the interferometer are proposed. Finally, a modified version of the equation relating the phase change with the overall interference state of the device is proposed, especially for the detection of biological agents. It is understood that the predictions provided by this equation may be overvalued. Nevertheless, we believe this equation has valuable scientific merits since it takes into account the shape and size of the BAs to detect.

8.0 REFERENCES

1. Kooyman, R. P., Kolkman, H., Van Gent, H., and Greve, J., "Surface Plasmon Resonance Immunosensors: Sensitivity Considerations", J. Anal. Chem. Acta, Vol. 213, 1988, pp. 33-45.

2. Cullen, D. C., Brown, R. G., and Lowe, C. R., "Detection of Immuno-Complex Formation via Surface Plasmon Resonance on Gold-Coated Diffraction Gratings", Biosensors, Vol. 3, 1988, pp. 211-225.

3. Goddard, N. J., Pollard-Knight, D., and Maule, C. H., "Real-time Biomolecular Interaction Analysis Using the Resonant Mirror", Analyst, Vol. 199, 1994, pp. 583-588.

4. Lee, W. E. and Thompson, H. G., "Detection of Newcastle Disease Virus using an Evanescent Wave Immuno-Based Biosensor", Can. J. Chem., Vol. 74, 1996, pp. 707-712.

5. Thompson, R. B. and Ligler, F. S., In "Biosensors with Fiber Optics", edited by D. L. Wise and L. B. Lwingard, Humana Press Inc., Clifton, N.J., 1991, pp. 111-138.

6. Tijssen, P., In "Practice and Theory of Enzyme Immunoassays", Elsevier, New York, 1985.

7. Lukosz, W., "Principles and Sensitivities of Integrated Optical and Surface Plasmon Sensors for Direct Affinity Sensing and Immunosensing", Biosensors and Bioelectronics, Vol. 6, 1991, pp. 215-225.

8. Flanagan, M. T., Sloper, A. N., and Ashworth, R. H., "From Electronic to Opto-Electronic Biosensors: an Engineering View", Analytica Chimica Acta, Vol. 213, 1988, pp. 23-33.

9. Gauglitz, G. and Ingenhoff, J., "Design of New Integrated Optical Substrates for Immuno-Analytical Applications", Fresenius J. Anal. Chem., Vol. 349, No. 5, 1994, pp. 355-359.

10. Boiarski, A. A., Busch, J. R., Bhullar, B. S., Ridgway, R. W., and Miller, L. S., "Integrated-Optic Biosensor", Proc. of SPIE Int. Soc. Opt. Eng.: Fiber Optic Sensors in Medical Diagnostics, Vol. 1886, 1993, pp. 15-26.

11. Hartman, N. F., Wyvill, J. C., Campbell, D. P. and Edmonds, P., "Rapid Response Biosensor for Detection and Identification of Common Foodborne Pathogens", Proc. of SPIE Int. Soc. Opt. Eng., Vol. 2345, 1995, pp. 128-137.

12. Snyder, A. W. and Love J. D., "Optical Waveguide Theory", Chapman & Hall, 1^{st} ed., New York, 1983.

13. Najafi, S. I., "Introduction to Glass Integrated Optics", Artech House, Inc., 1^{st} ed., Norwood, Massachusetts, 1992.

14. Alder, R. B., "Waves on Inhomogeneous Cylindrical Structures", Proc. I.R.E., Vol. 40, 1952, pp. 339-348.

15. Optonex Ltd., "Optonex Integrated Optics Design Software (PC/Windows environment)", Product information from company, Revontulentie 8 C, Espoo, Finland, November 1995, (Canadian representative: Guided Wave Technologies Inc.).

16. Heaton, H. I., "Thermal Straining in a Magnetostrictive Optical Fiber Interferometer", Applied Optics, Vol. 19, No. 22, 1980, p. 3719.

17. Yariv, A., "Proposal for Detection of Magnetic Fields through Magnetostrictive Perturbation of Optical Fibers", Optics Letters, Vol. 5, No. 3, 1980, p. 87.

18. Kolgenik, H., "Theory of Dielectric Waveguides", Topics in Applied Physics: Integrated Optics, Spinger-Verlag, Vol. 7, 1975, pp. 13-81.

19. Barnoski, M. K., "Introduction to Integrated Optics", Plenum Press, 1^{st} ed., New York, 1974.

20. Hariharan, P., "Optical Interferometry", Academic Press, 1^{st} ed., New York, 1985.

21. Françon, M., "Optical Interferometry", Academic Press, 1^{st} ed., New York, 1966, pp. 97-99.

22. Seastar Optics Inc., "Optical Devices & Laser Diode Instrumentation", Product catalog from company, 316 2^{nd} Ave. South, Seattle, Washington, 98104, USA, 1993, p. 37.

23. Weast, R. C., "CRC Handbook of Chemistry and Physics", CRC Press Inc., 68^{th} ed., Boca Raton, Florida, 1988, p. E-372.

24. Boiarski, A. A., Busch, J. R., Bhullar, B. S., Ridgway, R. W., and Wood, V., "Integrated-Optic Sensor with Macro-Flow Cell", Proc. of SPIE Int. Soc. Opt. Eng.: Integrated Optics and Microstructures, Vol. 1793, 1992, pp. 199-211.

INTERNAL DISTRIBUTION

DREV TM–9621

1 – Deputy Director General
1 – Chief Scientist
1 – H/ASSTA
6 – Document Library
1 – Jean-Robert Simard (coauthor)
1 – Deni Bonnier
1 – Vincent Larochelle
1 – Jim Cruickshank

EXTERNAL DISTRIBUTION

DREV TM–9621

2 – DRDIM
1 – CRAD

4 DRES:
– Attn: DRES library
– Dr. William E. Lee (coauthor)
– Dr. Greg Luoma
– Dr. John McFee

4 NDHQ:
– Attn: Mr. Dave Saint, DSAL 4
– Maj. D. B. Van Loon, DHO 4-3
– Maj. A. St-Onge, DSAHP 2
– LCol R.F. Carruthers, PD LAV (DLR 10)

2 École Polytechnique
Dept. Génie Physique
Case postale 6079, Succ. Centre-ville
Montréal, P.Q. H3C 3A7:
– Attn: Dr. Iraj Najafi and
– Dr. Ludvik Martinu

UNCLASSIFIED
SECURITY CLASSIFICATION OF FORM
(Highest classification of Title, Abstract, Keywords)

DOCUMENT CONTROL DATA

1. ORIGINATOR (name and address)

Defence Research Establishment Valcartier
P.O. Box 8800
Courcelette, P.Q.
Canada G0A 1R0

2. SECURITY CLASSIFICATION
(Including special warning terms if applicable)

UNCLASSIFIED

3. TITLE (Its classification should be indicated by the appropriate abbreviation (S,C,R or U)
Characterization of an Optically Integrated Mach-Zehnder Interferometer for the Detection of Biological Agents

4. AUTHORS (Last name, first name, middle initial. If military, show rank, e.g. Doe, Maj. John E.)

Dr. J.R. Simard (DREV) and Dr. William E. Lee (DRES)

5. DATE OF PUBLICATION (month and year)	6a. NO. OF PAGES	6b. NO. OF REFERENCES
April 1997	48	24

7. DESCRIPTIVE NOTES (the category of the document, e.g. technical report, technical note or memorandum. Give the inclusive dates when a specific reporting period is covered.)

Memorandum

8. SPONSORING ACTIVITY (name and address)

9a. PROJECT OR GRANT NO. (Please specify whether project or grant)	9b. CONTRACT NO.
Thrust 6EC21	

10a.ORIGINATOR'S DOCUMENT NUMBER	10b. OTHER DOCUMENT NOS.
	N/A

11. DOCUMENT AVAILABILITY (any limitations on further dissemination of the document, other than those imposed by security classification)

- [X] Unlimited distribution
- [ ] Contractors in appoved countries (specify)
- [ ] Canadian contractors (with need-to-know)
- [ ] Government (with need-to-know)
- [ ] Defence departments
- [ ] Other (please specify) :

12. DOCUMENT ANNOUNCEMENT (any limitation to the bibliographic announcement of this document. This will normally correspond to the Document Availability (11). However, where further distribution (beyond the audience specified in 11) is possible, a wider announcement audience may be selected.)

Unllimited

UNCLASSIFIED
SECURITY CLASSIFICATION OF FORM

13. ABSTRACT (a brief and factual summary of the document. It may also appear elsewhere in the body of the document itself. It is highly desirable that the abstract of classified documents be unclassified. Each paragraph of the abstract shall begin with an indication of the security classification of the information in the paragraph (unless the document itself is unclassified) represented as (S), (C), (R), or (U). It is not necessary to include here abstracts in both official languages unless the text is bilingual).

The process of environmental monitoring of biological agents is a major concern to the Canadian Forces and to the defence research community in general. The Canadian Integrated Biological Agent Detector System (CIBADS) and the Light Armoured Vehicle Reconnaissance (LAV RECCE) are two projects within the Department of National Defence where smaller, faster, and more sensitive biological detection technologies are of great interest for the integration of an efficient automated monitoring system for biological agents. A device that shows encouraging characteristics for this goal is a biorefractometer based on an integrated Mach-Zehnder interferometer. This document reports initial work to evaluate the capabilities of this device. A model relating the biological sensitivity of the device to its basic electro-optical properties is proposed. Also, the main parameters that may degrade the capacity of the detector are identified and quantified. Off-the-shelf interferometric waveguides were tested experimentally and compared successfully with the proposed model. From these experimental results, it was found that the minimum refractive index change measurable is comparable with the results published by other international scientific teams.

14. KEYWORDS, DESCRIPTORS or IDENTIFIERS (technically meaningful terms or short phrases that characterize a document and could be helpful in cataloguing the document. They should be selected so that no security classification is required. Identifiers, such as equipment model designation, trade name, military project code name, geographic location may also be included. If possible keywords should be selected from a published thesaurus. e.g. Thesaurus of Engineering and Scientific Terms (TEST) and that thesaurus-identified. If it is not possible to select indexing terms which are Unclassified, the classification of each sould be indicated as with the title.)

Biodetection
biotechnology
antibody
sensor
integrated optic
Mach-Zehnder
interferometer

UNCLASSIFIED

Requests for documents
should be sent to:

DIRECTORATE RESEARCH AND DEVELOPMENT
INFORMATION MANAGEMENT
Dept. of National Defence
Ottawa, Ontario
K1A 0K2

Tel.: (613) 995-2971
Fax: (613) 996-0392

502399

Toute demande de document
doit être adressée à:

DIRECTEUR-GESTION DE L'INFORMATION DE RECHERCHE
ET DE DÉVELOPPEMENT
Ministère de la Défense nationale
Ottawa, Ontario
K1A 0K2

Téléphone: (613) 995-2971
Télécopieur: (613) 996-0392

SANS CLASSIFICATION